Збірник наукових праць. Галузеве машинобудування, будівництво
Academic journal. Industrial Machine Building, Civil Engineering
http://journals.nupp.edu.ua/znp
https://doi.org/10.26906/znp.2025.64.4139

UDC 624.012.35

Oleg Kalmykov *
O. M. Beketov National University of Urban Economy in Kharkiv
https://orcid.org/0000-0001-7294-4279

Ivan Demianenko
O. M. Beketov National University of Urban Economy in Kharkiv
https://orcid.org/0000-0001-9511-7663

Sergei Potapov
O. M. Beketov National University of Urban Economy in Kharkiv
https://orcid.org/0009-0005-2845-4930

Dzhmaldii Alataev
O. M. Beketov National University of Urban Economy in Kharkiv
https://orcid.org/0000-0003-1570-8469

Strain Energy Density-Based Topology Optimization Using SIMP and Local Failure Criteria for 3D-Printed Concrete Structures

Abstract. This paper presents a strain energy density–based topology optimization method tailored for brittle materials such as 3D-printed concrete. Extending the SIMP framework, the approach incorporates a local failure criterion derived from a Lode–Nadai ultimate strain energy model, allowing each element to adapt to tension-, compression-, or shear-dominated stress states. A memory-locking mechanism preserves elements that exceed their local energy limits, preventing unstable material removal and improving structural robustness. The method is implemented in the FEniCS finite element environment, enabling full customization of material behavior and numerical routines. Benchmark simulations of a slab, cantilever beam, and foundation block demonstrate that the proposed strategy generates manufacturable, failure-resistant layouts and produces more physically consistent topologies than traditional compliance-based designs, particularly for materials with limited tensile capacity.

Keywords: topology optimization, simp, flat 3dcp, strain energy density, concrete.

*Corresponding author E-mail: oleg.kalmikov@kname.edu.ua

Received: 29.04.2025 Accepted: 03.06.2025 Published: 26.06.2025

Introduction.

Topology optimization has emerged as a powerful tool for designing high-performance structures by distributing material within a prescribed domain to achieve optimal mechanical behavior under given constraints. Among the various approaches, the Solid Isotropic Material with Penalization (SIMP) method is widely used due to its simplicity and ability to produce nearly discrete designs using continuous design variables [1,2]. However, conventional SIMP formulations primarily focus on compliance minimization, often neglecting the material's physical failure limits.

This limitation becomes critical in applications involving brittle or quasi-brittle materials - such as concreteespecially when used in additive manufacturing processes. In such contexts, mechanical failure is governed not only by stress magnitudes but also by the distribution and concentration of energy within the structure. Incorporating local failure criteria based on strain energy density offers a more physically meaningful way to guide material redistribution [3-5].

Strain energy density (SED) represents the internal elastic energy stored per unit volume and can serve as a valuable indicator for material failure, particularly when contrasted with the material's ultimate energy absorption capacity. By formulating the optimization process around an energy-based failure criterion, it becomes possible to ensure that all material in the structure remains within safe operating limits, enhancing structural robustness and reliability [6,7].

Recent advances in numerical extremum-search algorithms also emphasize the importance of energy-driven optimization principles. In particular, the improved Method of Integral Gradients (MIG) has demonstrated efficient procedures for locating global

extrema of multivariable functions [20,21], offering complementary perspectives that conceptually align with the strain-energy motivation adopted in this work.

Other studies have shown the effectiveness of iterative approaches for optimizing reinforced concrete floor systems, including early work on slab topology rationalization presented in [19].

This paper proposes an energy-constrained SIMP topology optimization framework where the optimization is driven by the ratio between the actual strain energy density and a local ultimate energy threshold. The threshold is computed using a Lode–Nadai-based formulation, where the ultimate energy is a function of the local deviatoric strain state. By using second-order polynomial interpolation of failure energies under uniaxial tension, compression, and pure shear, the model defines a continuous ultimate energy field that respects the material's multiaxial failure behavior [8,9].

An important aspect of the proposed framework is the spatially varying nature of the failure criterion, which reflects the multiaxial stress state of the structure. Moreover, a filtering strategy and preserved region constraints are introduced to prevent the formation of disconnected voids, promoting manufacturable and physically realistic structures. The method is particularly suitable for emerging materials and fabrication processes, such as 3D-printed concrete, where stress redistribution and material efficiency are paramount [10–12].

To demonstrate the effectiveness of the method, we apply it to three structural case studies: a cantilever beam, a foundation block with constrained supports, and a simply supported slab subjected to surface loads. Each example highlights the influence of the energy-based failure constraint on the topology evolution and final material layout.

The remainder of this paper introduces the theoretical basis of the strain-energy-driven failure criterion together with the Lode–Nadai interpolation, followed by a description of the proposed SIMP-based optimization framework and its numerical implementation. The subsequent sections present the topology optimization results for the selected case studies and conclude with key findings and prospects for future research.

Problem statement.

This study addresses the limitations of conventional SIMP-based topology optimization by integrating strain energy density constraints derived from Lode-Nadai strength theory. The goal is to ensure that each element remains within its mode-specific energy capacity while promoting structurally coherent and manufacturable designs.

Main material and results.

Overview and Physical Motivation. Topology optimization has become a fundamental tool in structural design, enabling the efficient distribution of material within a domain to maximize performance under constraints such as stiffness, mass, or manufacturing limits. While compliance minimization remains the prevailing objective in classical topology optimization [1], it often neglects local material failure risks. This is especially critical for brittle materials like 3D-printed concrete, where strain localization and cracking may occur well before global failure.

To address this, we propose a novel formulation of topology optimization that leverages local strain energy density as a governing criterion for material distribution. The method ensures that, throughout the optimization process, no element exceeds its allowable energy threshold derived from physically meaningful limits based on the Lode-Nadai failure model. This approach improves structural integrity by preventing weak internal zones and promoting manufacturable designs with well-defined stress trajectories [3,13].

The methodology is implemented using the SIMP (Solid Isotropic Material with Penalization) framework, enhanced with energy-based filtering and a memory mechanism to prevent reactivation of overloaded zones. The simulations are carried out using the open-source FEniCS computing platform [14], providing flexibility for integrating custom material models, solvers, and geometric definitions.

Strain Energy Density as a Failure Measure. Strain energy density w is an energy-based scalar field derived from the stress and strain tensors in the context of linear elasticity:

$$w = \frac{1}{2}\sigma : \varepsilon , \tag{1}$$

where $\boldsymbol{\sigma}$is the stress tensor and $\boldsymbol{\varepsilon}$the strain tensor. In topology optimization, the energy density provides a measure of local deformation and stress, making it a suitable candidate for evaluating the proximity to failure [15, 18].

To introduce failure sensitivity, we define a cell-wise ultimate strain energy threshold $e_u(\chi)$, determined as a function of the Lode-Nadai parameter $\chi \in [-1,1]$. This parameter captures the nature of the stress state - whether it is closer to uniaxial tension, compression, or shear – via the deviatoric strain invariants:

$$J_2 = \frac{1}{2}\mathrm{dev}(\boldsymbol{\varepsilon}) : \mathrm{dev}(\boldsymbol{\varepsilon}), J_3 = \det\left(\mathrm{dev}(\boldsymbol{\varepsilon})\right);$$
$$\chi = \frac{6}{\pi}\cdot\theta, \text{where } \sin(3\theta) = \frac{3\sqrt{3}}{2}\cdot\frac{J_3}{J_2^{3/2}} \tag{2}$$

We then define the energy threshold as a second-order polynomial in χ:

$$e_u(\chi) = \alpha_1 + \alpha_2\chi + \alpha_3\chi^2 . \tag{3}$$

The coefficients $\alpha_i$are computed from ultimate strain energies in three canonical stress states – uniaxial tension, uniaxial compression, and pure shear – using characteristic strengths of the 3D-printed concrete:

$$e_{btu} = \frac{R_{bt}^2}{2E}, e_{bcu} = \frac{R_b^2}{2E}, e_{bshu} = \frac{\tau_u^2}{2G}; \quad (4)$$

$$\alpha_1 = e_{bshu},$$
$$\alpha_2 = \frac{1}{2}\left(e_{bcu} - e_{btu}\right), \quad (5)$$
$$\alpha_3 = \frac{1}{2}\left(e_{bcu} + e_{btu}\right) - e_{bshu}.$$

This framework creates a spatially adaptive failure criterion, ensuring elements are not removed if they carry critical structural loads, even under varying local stress modes [16].

Numerical Implementation in FEniCS. The proposed method is implemented using the FEniCS finite element library [14], which offers efficient handling of variational problems in 3D domains. The workflow includes the following key elements:

- Mesh and Geometry: Domains are discretized using linear hexahedral elements (BoxMesh). For instance, the slab problem uses a grid of 255792 elements with a 0.04 m resolution in each direction.
- Function Spaces:
- Displacement field: Continuous Lagrange P1
- Density and energy fields: Discontinuous Galerkin DG0
- Boundary Conditions:
- Fixed support at bottom edges (100 mm wide band)
- Uniform vertical pressure load on top surface
  Material Parameters:
- Young's modulus $E = 30$GPa
- Poisson's ratio $\nu = 0.2$
- Tensile strength $R_{bt} = 3$MPa
- Compressive strength $R_b = 30$MPa

The solver employs the CG iterative method with AMG preconditioning, and each iteration includes full projection of energy fields and filtering.

SIMP Update Rule and Memory Locking. The density update follows the classical SIMP rule:

$$E(\rho) = E_0 \cdot \rho^p, \quad (6)$$

with penalization factor $p = 3$ and minimum density $\rho_{\min} = 0.001$. To avoid oscillatory behavior and to control convergence, we use a damped multiplicative update:

$$\rho^{(k+1)} = \text{clip}\left(\rho^{(k)} \cdot \left(\frac{\tilde{w}}{e_u(\chi)}\right)^{\eta}, \rho_{\min}, 1.0\right), \quad (7)$$

where $\tilde{w}$is a neighbor-averaged filtered strain energy and $\eta = 0.5$is the damping exponent.

To model irreversible failure, we introduce a damage memory mechanism: once an element exceeds its local threshold, it is locked at full density $\rho = 1$for all future iterations. This constraint stabilizes material redistribution and prevents premature deletion of structurally vital cells [17]. Figure 1 shows the full algorithm block-scheme.

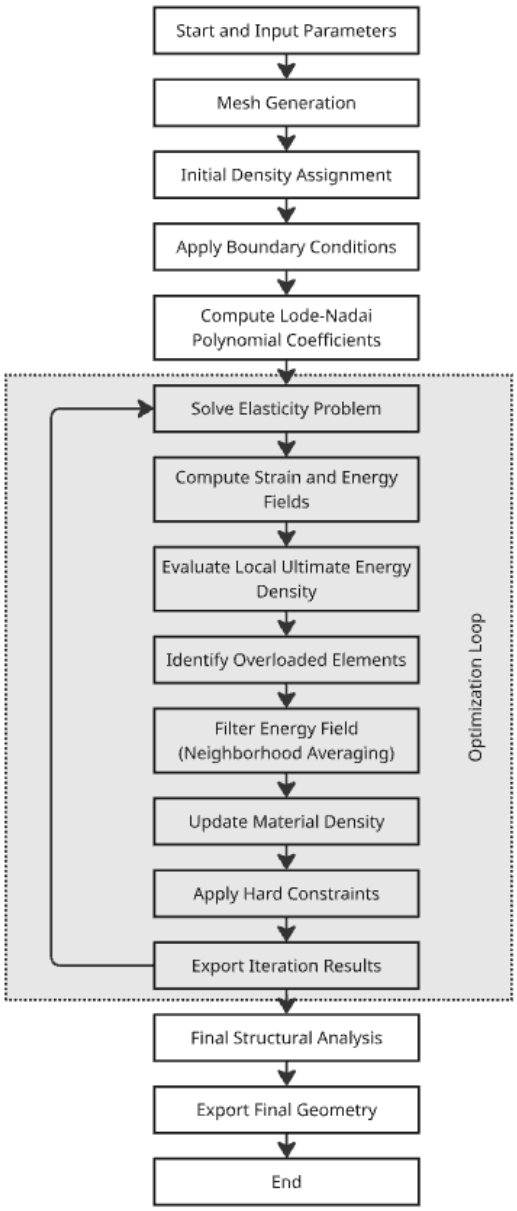

Figure 1 – Algorithm block-scheme

Simulation Results

Slab Under Uniform Load. A concrete slab of 2.2 m x 2.2 m plan dimensions and 0.24 m thickness was optimized under a uniformly distributed vertical pressure of 100 kPa acting on the entire top surface. The boundary conditions constrained a 100-mm band along the perimeter of the bottom surface, representing a stiffened support region that prevented displacement in all directions. All vertical and horizontal reactions were transferred through this preserved lower band, while the remaining internal volume of the slab was free to undergo topology optimization.

Under this loading–support configuration, the algorithm retained material in regions corresponding to dominant bending load paths. The most prominent retained feature is a continuous, fully preserved perimeter beam created by the enforced 100-mm outer band. This frame acts as the primary load-carrying

boundary and serves as the anchoring ring for internal stress redistribution.

Inside this perimeter, the optimization produced four distinct radial high-density zones located at the mid-span of each edge. These zones appear as denser, strip-like regions oriented approximately orthogonally to each side and directed toward the slab's centre. Their formation reflects the lines of principal bending and shear flow: under a uniform load with edge confinement, the mid-side regions carry significantly higher bending stresses than the corners. As a result, material accumulates along these mid-side stress trajectories, producing the characteristic "radial" ribs clearly visible in both top and bottom views.

In contrast, the corner regions exhibit noticeably lower density, indicating that they remain lightly stressed throughout loading. Optimization consistently clears material from these zones due to their reduced contribution to global stiffness. This creates a natural gradient from the preserved perimeter frame into sparsely populated corner volumes.

At the centre of the slab, the algorithm forms a compact rounded high-density core, which corresponds to the location of maximum bending moments under uniform surface pressure. Around this central region, the density gradually decreases, forming smooth transitions that resemble softly defined internal rings. These transitions highlight a typical bending-dominated response: high compressive and tensile strains concentrated near the slab's centre, with stresses diffusing outward toward the supporting boundaries.

The resulting topology therefore comprises:

- a fully preserved outer perimeter beam,
- four radial densification bands extending inward from each mid-side,
- low-density corner zones reflecting minimal strain demand, and
- a compact central dense area where bending stresses are greatest.

Overall, the optimized structure features realistic and manufacturable density gradients aligned directly with the mechanical behaviour of the slab under uniform loading and supported-edge boundary conditions. The final configuration efficiently concentrates material only where structurally required (see Figure 2).

The progression of material distribution and structural response over the 10 iterations is summarized in Table 1. As the optimization proceeded, the retained volume gradually decreased from 98.97% in the first iteration to 85.38% in the final iteration. This steady reduction reflects the removal of inefficient, lightly stressed material while maintaining stiffness-critical regions.

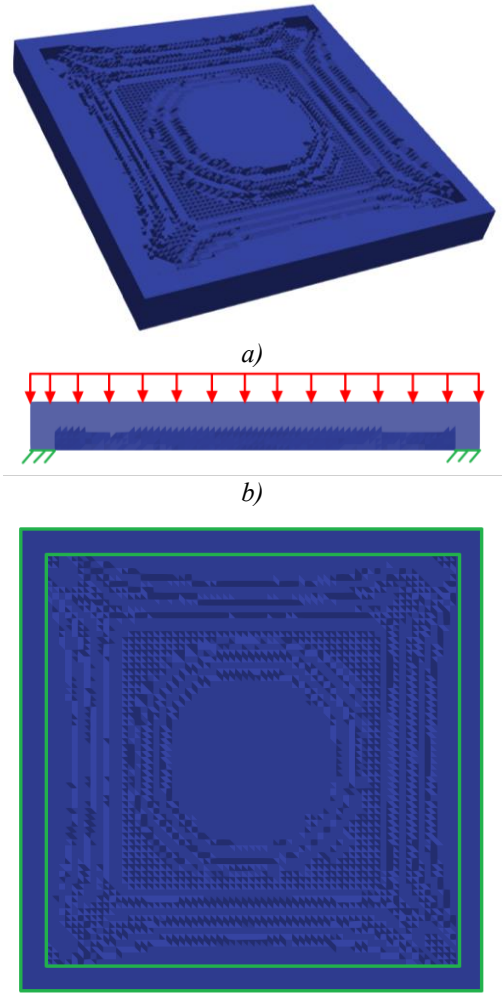

a)

b)

c)

Figure 2 – Topology of the bottom of the optimized slab: a) – 3D view of the bottom of the slab; b) – side view; c) - bottom view

Table 1 – Iteration-wise Optimization Metrics for the concrete slab

Iteration	Volume (%)	Avg SED (J/m³)	Max Principal Stress (MPa)	Max Principal Strain
0	98.97	7.645×10^{0}	1.207	3.678×10^{-5}
1	97.19	7.769×10^{0}	1.485	4.320×10^{-5}
2	95.72	7.856×10^{0}	1.417	4.101×10^{-5}
3	94.15	7.959×10^{0}	1.366	5.321×10^{-5}
4	92.61	8.058×10^{0}	1.301	4.455×10^{-5}
5	91.10	8.162×10^{0}	1.209	4.791×10^{-5}
6	89.64	8.263×10^{0}	1.199	5.736×10^{-5}
7	88.17	8.374×10^{0}	1.480	6.404×10^{-5}
8	86.74	8.479×10^{0}	1.318	7.858×10^{-5}
9	85.38	8.580×10^{0}	1.234	1.196×10^{-4}

Cantilever Beam. The 3.0 m cantilever beam, fixed at the left face and loaded on a small patch near the free end, developed a clear load-path-oriented internal structure after optimization. The clamped support region remained fully preserved, forming a stiff block that transfers all reactions into the boundary. From this support, the algorithm created a distinctive curved compression arch extending toward the loaded upper-

right zone, representing the principal compressive path under bending (Figure 3).

Below the compression arch, a large, elongated void emerged as low-strain-energy material was removed. The remaining shell-like rib structure follows the neutral axis and maintains global stiffness while significantly reducing volume. Along the tension side - primarily the lower surface - the optimization preserved slender diagonal ribs aligned with the principal tensile strain directions, forming an organic truss-like network characteristic of bending-dominated members.

Near the load application region, material condensed into a local node that distributes the applied pressure into the surrounding arch and tension ribs. The preservation of this zone ensures realistic load transfer and avoids localized overstress.

Overall, the final topology consists of a stiff support block, a dominant compression arch, a tension rib network, and a central void created by material removal. This configuration captures the classic structural behavior of a cantilever under tip loading, with material placed efficiently along principal stress trajectories (see Figure 3).

The evolution of material distribution and mechanical response over the iterations is summarized in Table X. As the optimization progressed, the retained volume decreased from 66.87% in the first iteration to 48.60% in the final iteration, while the average strain energy stabilized around 5×10^3 J/m³. Maximum principal stresses ranged between 49–135 MPa, reflecting shifts in load paths as nonessential material was removed. Despite the significant mass reduction, the topology preserved global stiffness by concentrating material precisely along the principal compression and tension trajectories.

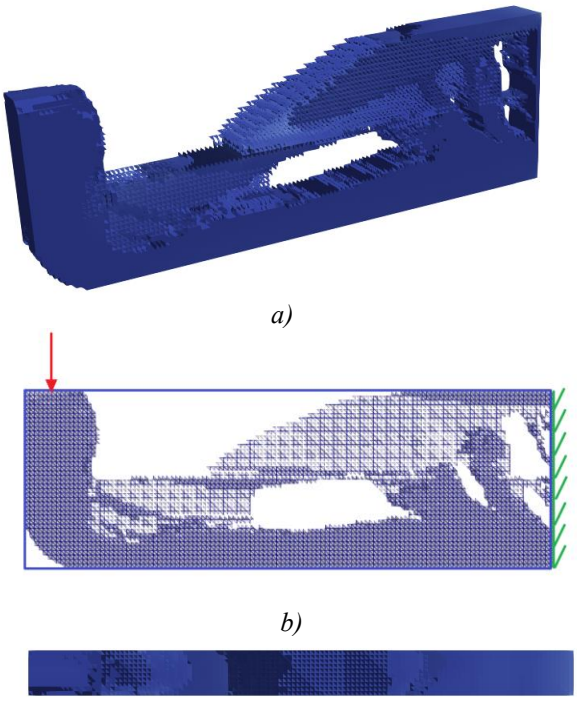

a)

b)

c)

Figure 3 – Topology of the optimized cantilever beam: a) – 3D view; b) – side view; c) – top view

Table 2 – Iteration-wise Optimization Metrics for the concrete slab

Iteration	Volume (%)	Avg SED (J/m³)	Max Principal Stress (MPa)	Max Principal Strain (–)
0	66.87	1.826×10^3	49.28	1.558×10^{-3}
1	56.34	6.278×10^3	81.02	8.153×10^{-3}
2	57.69	7.862×10^3	102.3	6.298×10^{-2}
3	55.45	6.408×10^3	114.3	6.203×10^{-2}
4	53.50	5.414×10^3	118.7	5.511×10^{-2}
5	51.56	5.135×10^3	120.6	5.164×10^{-2}
6	50.20	5.049×10^3	120.5	3.627×10^{-2}
7	49.35	5.025×10^3	120.3	6.618×10^{-2}
8	48.89	5.028×10^3	122.0	5.651×10^{-2}
9	48.60	5.037×10^3	134.7	3.283×10^{-2}

Foundation Block. The 1.18 m × 0.60 m × 0.58 m foundation block was optimized under a vertical uniformly distributed load applied over the entire top surface, while the bottom boundary was fully constrained to mimic ground contact. A 100 mm thick exterior shell was preserved along all faces, leaving only the interior core free for material removal. This setup reproduces a realistic foundation condition in which the outer concrete envelope must remain solid for constructability, durability, and anchorage, while the inner volume is optimized for structural efficiency (Figure 4).

Under these boundary conditions, the optimization produced a compact internal load-bearing structure aligned with the primary vertical compression flow. Instead of forming a single large void, the interior developed two dominant vertical compression columns, located near the left and right thirds of the block (Figure 4). These zones correspond to regions where strain energy remained highest during the iteration. Between these columns, the optimizer removed material extensively, creating a central horizontal cavity where strain energy levels were consistently low. This cavity formed without compromising global stiffness because the preserved outer shell and vertical internal ribs-maintained continuity of load transfer.

The resulting topology resembles a dual-column strut system embedded inside the shell, with the preserved exterior surfaces acting as a stiff frame surrounding a lighter internal structure (Figures 4). The inner ribs and columns are oriented in the direction of principal compressive stresses, forming organic, branching load paths rather than orthogonal grid patterns. This behavior is characteristic of strain-energy-based optimization methods, which tend to form compression trees rather than predefined truss geometries.

Near the top surface, material was retained over a broad area to distribute the applied pressure into the internal columns, avoiding localized overstress. At the bottom, the preserved shell concentrated stiffness along the support plane, ensuring uniform transfer of reaction forces into the ground. As iterations progressed, the optimizer reduced the density of peripheral interior regions, producing a smooth transition from dense vertical struts to the central cavity.

Overall, the optimized foundation block demonstrates a structurally efficient internal load-bearing topology: a preserved stiff outer shell enclosing two major compression struts and several secondary ribs, all aligned with principal compressive stress trajectories. This configuration provides a significant mass reduction in the core while maintaining the load-carrying capacity required under uniform vertical compression (Figures 4).

As the optimization progressed, the interior volume fraction decreased steadily - from 97.90% in the initial iteration to 88.69% by iteration 9 - indicating gradual removal of low-contributing material while maintaining the global load-bearing framework. Meanwhile, the average strain energy density increased slightly, stabilizing around 1.23×10^{1} J/m³, reflecting a more efficient internal stress distribution. Maximum principal stresses increased from 0.026 MPa to 0.478 MPa as material concentrated along narrower load paths, consistent with strut formation. These trends are summarized in Table X.

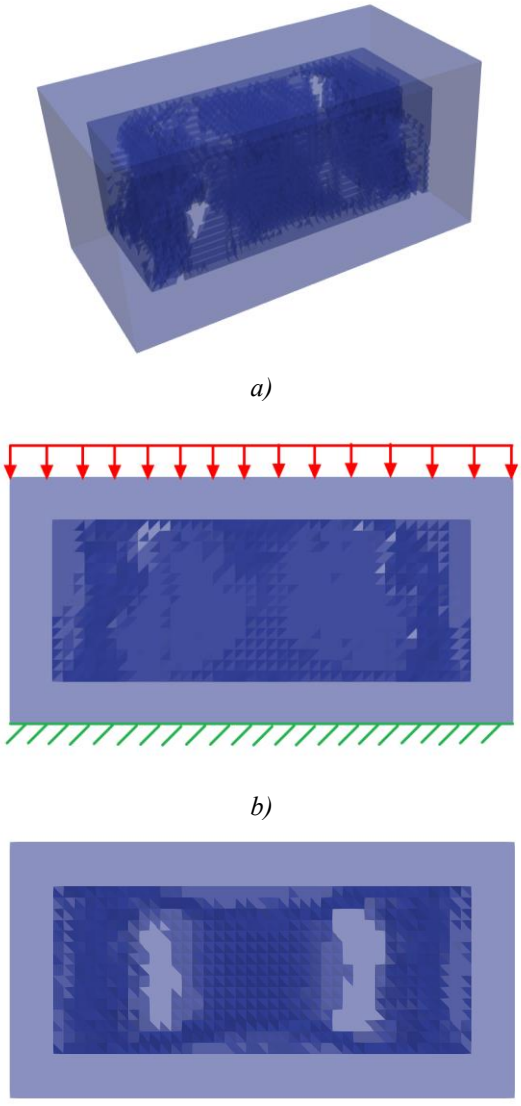

a)

b)

c)

Figure 4 – Topology of the optimized foundation block: a) – 3D view; b) – side view; c) – top view

Table 2 – Iteration-wise Optimization Metrics for the concrete block

Iteration	Volume (%)	Avg SED (J/m³)	Max principal stress (MPa)	Max principal strain (–)
0	97.90	1.046×10^{1}	0.026	8.490×10^{-6}
1	96.97	1.151×10^{1}	0.392	2.082×10^{-5}
2	96.50	1.156×10^{1}	0.407	3.101×10^{-5}
3	95.84	1.165×10^{1}	0.435	3.376×10^{-5}
4	94.05	1.177×10^{1}	0.463	4.107×10^{-5}
5	91.92	1.191×10^{1}	0.460	6.222×10^{-5}
6	90.67	1.206×10^{1}	0.446	7.625×10^{-5}
7	89.66	1.218×10^{1}	0.449	5.373×10^{-5}
8	89.07	1.227×10^{1}	0.451	6.290×10^{-5}
9	88.69	1.235×10^{1}	0.478	7.823×10^{-5}

Each test case converged within 10 iterations. No checkerboarding or disconnected regions were observed, confirming the method's robustness for practical structural configurations.

Conclusions.

This work introduced a strain energy density-based topology optimization framework that combines SIMP penalization with a Lode-Nadai-derived multiaxial energy limit. The method incorporates a stability-oriented memory mechanism and preserves manufacturable outer boundaries, making it suitable for brittle and additively manufactured concrete structures.

Across all numerical examples, the approach produced stable, continuous, and mechanically meaningful topologies. The optimized structures demonstrated material reduction between approximately 10–50%, depending on boundary conditions, while maintaining coherent load paths across 10 sample iterations. The strain-energy redistribution observed during iteration showed consistent trends: average SED increased modestly, while maximum stress values rose as material concentrated along principal trajectories, reflecting improved structural efficiency rather than numerical instability. These behaviors were consistent across bending, compression, and combined-stress configurations.

Importantly, the method avoided checkerboarding and maintained connectivity without artificial filters. The internal topologies - central cavities, strut-like compression ribs, and stress-aligned bending members emerged naturally from the energy criterion, confirming that the formulation captures true mechanical behavior rather than numerical artifacts.

Overall, the results demonstrate that incorporating multiaxial strain-energy limits into SIMP leads to topologies that are efficient, realistic, and suitable for 3D-printed concrete applications. The framework provides a foundation for future developments, including nonlinear constitutive modeling, anisotropic printing constraints, and integration with AI-assisted optimization workflows.

References

1. Bendsøe, M. P., & Sigmund, O. (2003). *Topology Optimization: Theory, Methods, and Applications*. Springer. https://doi.org/10.1007/978-3-662-05086-6
2. Sigmund, O., & Maute, K. (2013). Topology optimization approaches. *Structural and Multidisciplinary Optimization*, 48(6), 1031–1055. https://doi.org/10.1007/s00158-013-0978-6
3. Rozvany, G. I. N. (2009). A critical review of established methods of structural topology optimization. *Structural and Multidisciplinary Optimization*, 37(3), 217–237. https://doi.org/10.1007/s00158-009-0464-8
4. Ghaffari, M., & Maroufi, S. (2020). A stress-constrained topology optimization method based on energy equivalence. *Engineering Optimization*, 52(6), 987–1004. https://doi.org/10.1080/0305215X.2019.1646975
5. Nguyen, D. D., Bruns, T. E., & Tortorelli, D. A. (2010). Stress-based topology optimization for continua. *Structural and Multidisciplinary Optimization*, 42(4), 591–604. https://doi.org/10.1007/s00158-010-0565-6
6. Lian, J., Luo, Y., & Huang, X. (2021). Topology optimization using strain energy density and failure index constraints. *Materials & Design*, 197, 109233. https://doi.org/10.1016/j.matdes.2020.109233
7. Luo, Y., & Kang, Z. (2022). Stress-constrained topology optimization using energy-based failure criteria. *Computer Methods in Applied Mechanics and Engineering*, 390, 114536. https://doi.org/10.1016/j.cma.2021.114536
8. Nadai, A. (1950). *Theory of Flow and Fracture of Solids*. McGraw-Hill.
9. You, F., & Chen, L. (2015). A novel energy-based failure criterion for quasi-brittle materials. *International Journal of Solids and Structures*, 58, 107–117. https://doi.org/10.1016/j.ijsolstr.2014.11.003
10. Panda, B., & Tan, M. J. (2018). Experimental study on mix proportion and fresh properties of fly ash based geopolymer for 3D concrete printing. *Ceramics International*, 44(9), 10258–10265. https://doi.org/10.1016/j.ceramint.2018.03.184
11. Ma, G., & Wang, L. (2018). A critical review of preparation design and workability measurement of concrete material for large-scale 3D printing. *Frontiers of Structural and Civil Engineering*, 12(3), 382–400. https://doi.org/10.1007/s11709-018-0482-6
12. Hambach, M., & Volkmer, D. (2017). Properties of 3D-printed fiber-reinforced Portland cement paste. *Cement and Concrete Composites*, 79, 62–70. https://doi.org/10.1016/j.cemconcomp.2017.02.007
13. Li, J., Liang, H., Zhang, D., & Zhao, J. (2022). A Lode-angle dependent criterion for concrete failure under 3D stress states. *Engineering Fracture Mechanics*, 268, 108453. https://doi.org/10.1016/j.engfracmech.2022.108453
14. Alnæs, M. S., et al. (2015). The FEniCS project version 1.5. *Archive of Numerical Software*, 3(100), 9–23. https://doi.org/10.11588/ans.2015.100.20553
15. Kohn, R. V., & Strang, G. (1986). Optimal design and relaxation of variational problems. *Communications on Pure and Applied Mathematics*, 39(1), 113–137. https://doi.org/10.1002/cpa.3160390109
16. Nguyen, T., & Paulino, G. H. (2017). Strain-based formulation for topology optimization with material failure constraints. *Computer Methods in Applied Mechanics and Engineering*, 318, 785–810. https://doi.org/10.1016/j.cma.2017.03.023

1. Bendsøe, M. P., & Sigmund, O. (2003). *Topology Optimization: Theory, Methods, and Applications*. Springer. https://doi.org/10.1007/978-3-662-05086-6
2. Sigmund, O., & Maute, K. (2013). Topology optimization approaches. *Structural and Multidisciplinary Optimization*, 48(6), 1031–1055. https://doi.org/10.1007/s00158-013-0978-6
3. Rozvany, G. I. N. (2009). A critical review of established methods of structural topology optimization. *Structural and Multidisciplinary Optimization*, 37(3), 217–237. https://doi.org/10.1007/s00158-009-0464-8
4. Ghaffari, M., & Maroufi, S. (2020). A stress-constrained topology optimization method based on energy equivalence. *Engineering Optimization*, 52(6), 987–1004. https://doi.org/10.1080/0305215X.2019.1646975
5. Nguyen, D. D., Bruns, T. E., & Tortorelli, D. A. (2010). Stress-based topology optimization for continua. *Structural and Multidisciplinary Optimization*, 42(4), 591–604. https://doi.org/10.1007/s00158-010-0565-6
6. Lian, J., Luo, Y., & Huang, X. (2021). Topology optimization using strain energy density and failure index constraints. *Materials & Design*, 197, 109233. https://doi.org/10.1016/j.matdes.2020.109233
7. Luo, Y., & Kang, Z. (2022). Stress-constrained topology optimization using energy-based failure criteria. *Computer Methods in Applied Mechanics and Engineering*, 390, 114536. https://doi.org/10.1016/j.cma.2021.114536
8. Nadai, A. (1950). *Theory of Flow and Fracture of Solids*. McGraw-Hill.
9. You, F., & Chen, L. (2015). A novel energy-based failure criterion for quasi-brittle materials. *International Journal of Solids and Structures*, 58, 107–117. https://doi.org/10.1016/j.ijsolstr.2014.11.003
10. Panda, B., & Tan, M. J. (2018). Experimental study on mix proportion and fresh properties of fly ash based geopolymer for 3D concrete printing. *Ceramics International*, 44(9), 10258–10265. https://doi.org/10.1016/j.ceramint.2018.03.184
11. Ma, G., & Wang, L. (2018). A critical review of preparation design and workability measurement of concrete material for large-scale 3D printing. *Frontiers of Structural and Civil Engineering*, 12(3), 382–400. https://doi.org/10.1007/s11709-018-0482-6
12. Hambach, M., & Volkmer, D. (2017). Properties of 3D-printed fiber-reinforced Portland cement paste. *Cement and Concrete Composites*, 79, 62–70. https://doi.org/10.1016/j.cemconcomp.2017.02.007
13. Li, J., Liang, H., Zhang, D., & Zhao, J. (2022). A Lode-angle dependent criterion for concrete failure under 3D stress states. *Engineering Fracture Mechanics*, 268, 108453. https://doi.org/10.1016/j.engfracmech.2022.108453
14. Alnæs, M. S., et al. (2015). The FEniCS project version 1.5. *Archive of Numerical Software*, 3(100), 9–23. https://doi.org/10.11588/ans.2015.100.20553
15. Kohn, R. V., & Strang, G. (1986). Optimal design and relaxation of variational problems. *Communications on Pure and Applied Mathematics*, 39(1), 113–137. https://doi.org/10.1002/cpa.3160390109
16. Nguyen, T., & Paulino, G. H. (2017). Strain-based formulation for topology optimization with material failure constraints. *Computer Methods in Applied Mechanics and Engineering*, 318, 785–810. https://doi.org/10.1016/j.cma.2017.03.023

17. Wang, M. Y., Wang, X., & Guo, D. (2003). A level set method for structural topology optimization. *Computer Methods in Applied Mechanics and Engineering*, 192(1), 227–246. https://doi.org/10.1016/S0045-7825(02)00585-8

18. Шмуклер В.С. (2017). Нові енергетичні принципи раціоналізації конструкцій. *Збірник наукових праць Українського державного університету залізничного транспорту*, *167*, 54-69. https://doi.org/10.18664/1994-7852.167.2017.97206

19. Калмиков О.О., Резнік П.А., В'юнковський В.П., Дем'яненко І.М., Булдаков О.О. (2025). Про пошук оптимальної топології залізобетонної плити перекриття. *Комунальне господарство міст*, 4(192), 228–235. https://doi.org/10.33042/3083-6727-2025-4-192-228-235

20. Kovalenko, L., Kalmykov, O., Reznik, P., & Demianenko, I. (2023). Numerical implementation of multidimensional functions extremum search. *Lecture Notes in Networks and Systems*, 807, 82–94. https://doi.org/10.1007/978-3-031-46874-2_8

21. Shmukler, V., Babaev, V., Kovalenko, L., Kalmykov, O., & Demianenko, I. (2023). Method of integral gradients for searching global extremum of multivariable functions (procedure improvement). *Lecture Notes in Networks and Systems*, 807, 71–81. https://doi.org/10.1007/978-3-031-46874-2_7

17. Wang, M. Y., Wang, X., & Guo, D. (2003). A level set method for structural topology optimization. *Computer Methods in Applied Mechanics and Engineering*, 192(1), 227–246. https://doi.org/10.1016/S0045-7825(02)00585-8

18. Shmukler, V.S. (2017). New Energy Principles of Structural Rationalization. *Collection of Scientific Papers of the Ukrainian State University of Railway Transport*, 167, 54–69. https://doi.org/10.18664/1994-7852.167.2017.97206

19. Kalmykov O.O., Reznik P.A., Viunkovskyi V.P., Demianenko I.M., Buldakov O.O. (2025). Pro poshuk optimalnoi topolohii zalizobetonnoi plyty perekryttia. *Municipal economy of cities.* ***192(4)****, 228–235.* https://doi.org/10.33042/3083-6727-2025-4-192-228-235

20. Kovalenko, L., Kalmykov, O., Reznik, P., & Demianenko, I. (2023). Numerical implementation of multidimensional functions extremum search. *Lecture Notes in Networks and Systems*, 807, 82–94. https://doi.org/10.1007/978-3-031-46874-2_8

21. Shmukler, V., Babaev, V., Kovalenko, L., Kalmykov, O., & Demianenko, I. (2023). Method of integral gradients for searching global extremum of multivariable functions (procedure improvement). *Lecture Notes in Networks and Systems*, 807, 71–81. https://doi.org/10.1007/978-3-031-46874-2_7

Suggested Citation:

APA style: Kalmykov, O., Demianenko, I., Potapov, S., & Alataev, D. (2025). Strain Energy Density-Based Topology Optimization Using SIMP and Local Failure Criteria for 3D-Printed Concrete Structures. *Academic Journal Industrial Machine Building Civil Engineering*, *1* (64), 80–88. https://doi.org/10.26906/znp.2025.64.4139

DSTU style: Strain Energy Density-Based Topology Optimization Using SIMP and Local Failure Criteria for 3D-Printed Concrete Structures/ O. Kalmykov et al. *Academic journal. Industrial Machine Building, Civil Engineering.* 2025. Vol. 64, iss. 1. P. 80–88. URL: https://doi.org/10.26906/znp.2025.64.4139.

Калмиков О.О.*
Харківський національний університет міського господарства імені О. М. Бекетова
https://orcid.org/0000-0003-2214-3128

Дем'яненко І.М.
Харківський національний університет міського господарства імені О. М. Бекетова
https://orcid.org/0000-0002-5654-5849

Потапов С.А.
Харківський національний університет міського господарства імені О. М. Бекетова
https://orcid.org/0009-0005-2845-4930

Алатаєв Д.А.
Харківський національний університет міського господарства імені О. М. Бекетова
https://orcid.org/0000-0003-1570-8469

Оптимізація топології на основі густини енергії деформації із використанням SIMP та локальних критеріїв руйнування для конструкцій із бетону, надрукованого методом 3D-друку

Аннотація. У статті запропоновано метод оптимізації топології крихких матеріалів на основі густини енергії деформації, з орієнтацією на застосування до бетонних конструкцій, виготовлених методом 3D-друку. На основі підходу SIMP (ізотропний твердий матеріал з пеналізацією), метод інтегрує локальний критерій руйнування, побудований на моделі граничної енергії деформації типу Лоде–Надаі. Запропонований критерій враховує напружений стан через девіаторні інваріанти деформацій, що дозволяє адаптуватися до умов розтягування, стиску чи зсуву на рівні окремих елементів сітки. Уведено механізм «блокування пам'яті», який незворотно зберігає ті елементи, що перевищили локальний поріг граничної енергії, що забезпечує конструктивну надійність і запобігає нестабільному видаленню матеріалу. Чисельна реалізація виконана у середовищі скінченних елементів FEniCS, що забезпечує повну гнучкість у визначенні матеріальних моделей та алгоритмів розв'язання. Продемонстровано ефективність методу на прикладі плити, консольної балки та фундаментного блоку — оптимізовані конфігурації забезпечують реалізовані конструкції зі зменшеним об'ємом матеріалу і підвищеною стійкістю до руйнування. Результати свідчать про те, що енергетичний підхід дозволяє отримувати більш фізично обґрунтовані рішення порівняно з традиційною оптимізацією за критерієм комплаєнсу, особливо для матеріалів із низькою міцністю на розтяг.

Ключові слова: топологічна оптимізація, SIMP, 3D-друк з бетону, щільність енергії деформації, бетон.

*Адреса для листування E-mail: oleg.kalmikov@kname.edu.ua

Надіслано до редакції:	29.04.2025	Прийнято до друку після рецензування:	03.06.2025	Опубліковано (оприлюднено):	26.06.2025